CMS Physics Analysis Summary

Contact: cms-pag-conveners-exotica@cern.ch 2017/03/24

Searches for dijet resonances in pp collisions at $\sqrt{s} = 13$ TeV using data collected in 2016

The CMS Collaboration

Abstract

Searches are presented for narrow resonances decaying to dijet final states in proton-proton collisions at $\sqrt{s} = 13$ TeV. A low-mass search, for a resonance mass between 0.6 TeV and 1.6 TeV, is performed using dijets that are reconstructed from calorimeter information in the trigger using data corresponding to an integrated luminosity of 27 fb^{-1}. A high-mass search, for resonances with mass above 1.6 TeV, is performed using dijets reconstructed with the particle flow algorithm from the normal reconstruction chain using data corresponding to an integrated luminosity of 36 fb^{-1}. The dijet mass spectrum is well described by a smooth parameterization and no significant evidence for the production of new particles is observed. Upper limits at 95% confidence level are reported on the production cross section for narrow resonances with masses above 0.6 TeV. In the context of specific models, the limits exclude string resonances with masses below 7.7 TeV, scalar diquarks below 7.2 TeV, axigluons and colorons below 6.1 TeV, excited quarks below 6.0 TeV, color-octet scalars below 3.4 TeV, W′ bosons below 3.3 TeV, Z′ bosons below 2.7 TeV, RS gravitons below 1.7 TeV and between 2.1 and 2.5 TeV, and dark matter mediators below 2.6 TeV. The limits on both vector and axial-vector mediators, in a simplified model of interactions between quarks and dark matter, are also presented as functions of dark matter mass. These extend previous limits in the dijet channel.

1 Introduction

The dijet mass (m_{jj}) spectrum in proton-proton (pp) collisions arising from the production of partons at high transverse momentum (p_T) is predicted by quantum chromodynamics (QCD) to fall smoothly with increasing dijet mass. Many models of physics beyond the standard model (SM) require new particles that couple to quarks (q) and gluons (g) and can be observed as resonances in the dijet mass spectrum. One example is a model in which dark matter (DM) particles couple to quarks through a DM mediator. This mediator can decay to either a pair of DM particles or a pair of jets and therefore can be observed as a dijet resonance [1]. Here, we report a search for narrow dijet resonances, which are those with natural widths that are small compared to the experimental mass resolution.

This analysis summary presents the results of two searches for dijet resonances, using pp collisions at $\sqrt{s} = 13\,\text{TeV}$ collected in 2016 with the CMS detector at the CERN LHC. The first is a *low-mass* search for resonances with mass between 0.6 and 1.6 TeV using dijet events corresponding to an integrated luminosity of $27\,\text{fb}^{-1}$. The events are reconstructed, selected, and recorded in a compact form by the high-level trigger (HLT) in a technique called *data scouting* [2]. Data scouting was previously used for low-mass searches published by CMS at $\sqrt{s} = 13\,\text{TeV}$ [3] and $\sqrt{s} = 8\,\text{TeV}$ [4], and is similar to a trigger level search at $\sqrt{s} = 13\,\text{TeV}$ reported by ATLAS [5]. The second is a *high-mass* search for resonances with mass above 1.6 TeV using dijet events that are reconstructed offline corresponding to an integrated luminosity of $36\,\text{fb}^{-1}$. Similar high-mass searches were published by CMS and ATLAS at $\sqrt{s} = 13\,\text{TeV}$ [3, 6, 7], 8 TeV [8–10], and 7 TeV [11–17] using strategies reviewed in Ref. [18]. The most recently reported high-mass searches used data collected in 2016 corresponding to an integrated luminosity of $12.9\,\text{fb}^{-1}$ by CMS [3] and $15.7\,\text{fb}^{-1}$ by ATLAS [19].

We present model-independent results and, in addition, consider the following benchmark models of s-channel dijet resonances: string resonances [20, 21], scalar diquarks [22], axigluons [23, 24], colorons [24, 25], excited quarks (q^*) [26, 27], color-octet scalars [28], new gauge bosons (W' and Z') with SM-like or leptophobic couplings [29], DM mediators [30, 31], and Randall–Sundrum (RS) gravitons (G) [32]. The specific choices of parameters for the benchmark models are the same as those that were used in the previous CMS search [3]. In the color-octet scalar model the squared anomalous coupling used is $k_s^2 = 1/2$ [33], and for the RS Graviton model the coupling used is $k/M_{PL} = 0.1$. For the DM mediator we follow the recommendations of Ref. [30] on model choice and coupling values, using a simplified model [31] of a spin-1 mediator decaying only to $q\bar{q}$ and pairs of DM particles, with unknown mass m_{DM}, and with a universal quark coupling $g_q = 0.25$ and a DM coupling $g_{DM} = 1.0$.

2 Jet reconstruction and event selection

The CMS detector and its coordinate system, including the azimuthal angle ϕ and the pseudorapidity η, are described in detail in Ref. [34]. The central feature of the CMS apparatus is a superconducting solenoid of 6 m internal diameter providing an axial field of 3.8 T. Within the field volume are located the silicon pixel and strip tracker ($|\eta| < 2.4$) and the barrel and endcap calorimeters ($|\eta| < 3$), which consist of a lead tungstate crystal electromagnetic calorimeter, and a brass and scintillator hadron calorimeter. An iron and quartz-fiber hadron calorimeter is located in the forward region ($3 < |\eta| < 5$), outside the field volume.

A particle-flow (PF) event algorithm reconstructs and identifies each individual particle with an optimized combination of information from the various elements of the CMS detector [35, 36]. Particles are classified as muons, electrons, photons, and either charged or neutral hadrons.

Jets are reconstructed either using particle flow, giving *PF-jets*, or from energy deposits in the calorimeters, giving *Calo-jets*. PF-jets reconstructed offline are used in the high-mass search, and Calo-jets reconstructed by the HLT are used in the low-mass search. To reconstruct both types of jets, we use the anti-k_T algorithm [37, 38] with a distance parameter of 0.4, as implemented in the FASTJET package [39]. For the high-mass search, at least one reconstructed vertex is required. The primary vertex is defined as the vertex with the highest sum of p_T^2 of the associated tracks. For PF-jets, charged PF candidates not originating from the primary vertex are removed prior to the jet finding. For both types of jets, an event-by-event correction based on jet area [40, 41] is applied to the jet energy to remove the estimated contribution from additional collisions in the same or adjacent bunch crossings (pileup).

Events are selected using a two-tier trigger system. Events satisfying loose jet requirements at the first level (L1) are examined by the HLT. The HLT uses H_T, the scalar sum of the jet p_T from all jets in the event with $|\eta| < 3$ that satisfy a jet p_T requirement, to select events. For the high-mass search, PF-jets with $p_T > 30\,\text{GeV}$ are used to compute H_T, and events are accepted by the HLT if they satisfy either the requirement $H_T > 900\,\text{GeV}$ or pass other triggers requiring a high p_T jet. We then select events with $m_{jj} > 1.25\,\text{TeV}$ for which the combined L1 trigger and HLT are found to be fully efficient for the full $36\,\text{fb}^{-1}$ sample. For the low-mass search, when an event passes the HLT, the Calo-jets reconstructed at the HLT are saved, along with the event energy density and missing transverse momentum reconstructed from the calorimeter. The shorter time for event reconstruction of calorimeter quantities and the reduced event size recorded for these events allow a reduced H_T threshold compared to the high-mass search. For the low-mass search, Calo-jets with $p_T > 40\,\text{GeV}$ are used to compute H_T, the threshold is $H_T > 250\,\text{GeV}$, and we select events with $m_{jj} > 0.49\,\text{TeV}$ for which the trigger is fully efficient. Only the first $27\,\text{fb}^{-1}$ of integrated luminosity was used for the low-mass search, due to an inefficiency in the L1 jet H_T trigger at the end of the run.

The jet momenta and energies are corrected using calibration constants obtained from simulation, test beam results, and pp collision data at $\sqrt{s} = 13\,\text{TeV}$. The methods described in Ref. [41] are used and all *in-situ* calibrations are obtained from the current data. All jets are required to have $p_T > 30\,\text{GeV}$ and $|\eta| < 2.5$. The two jets with largest p_T are defined as the leading jets. Jet identification (ID) criteria are applied to remove spurious jets associated with calorimeter noise. The jet ID for PF-jets is described in Ref. [42]. The jet ID for Calo-jets requires that the jet be detected by both the electromagnetic and hadronic calorimeters with the fraction of jet energy deposited within the electromagnetic calorimeter between 5% and 95% of the total jet energy. An event is rejected if either of the two leading jets fails the jet ID criteria.

Spatially close jets are combined into "wide jets" and used to determine the dijet mass, as in the previous CMS searches [8, 10, 11, 14]. The wide-jet algorithm, designed for dijet resonance event reconstruction, reduces the analysis sensitivity to gluon radiation from the final-state partons. The two leading jets are used as seeds and the four-vectors of all other jets, if within $\Delta R = \sqrt{(\Delta\eta)^2 + (\Delta\phi)^2} < 1.1$, are added to the nearest leading jet to obtain two wide jets, which then form the dijet system. The background from t-channel dijet events peaks at large values of $|\Delta\eta_{jj}|$ and is suppressed by requiring the pseudorapidity separation of the two wide jets to satisfy $|\Delta\eta_{jj}| < 1.3$. The above requirements maximize the search sensitivity for isotropic decays of dijet resonances in the presence of QCD dijet background. For the low-mass search, after wide jet reconstruction and event selection, we use a correction derived from a smaller sample of dijet data to calibrate the wide jets reconstructed from Calo-jets at HLT. With this correction, based on a dijet balance tag-and-probe method similar to that discussed in Ref. [41], the wide jets from Calo-jets have the same response as those reconstructed from PF-jets.

3 Dijet mass spectrum and fit

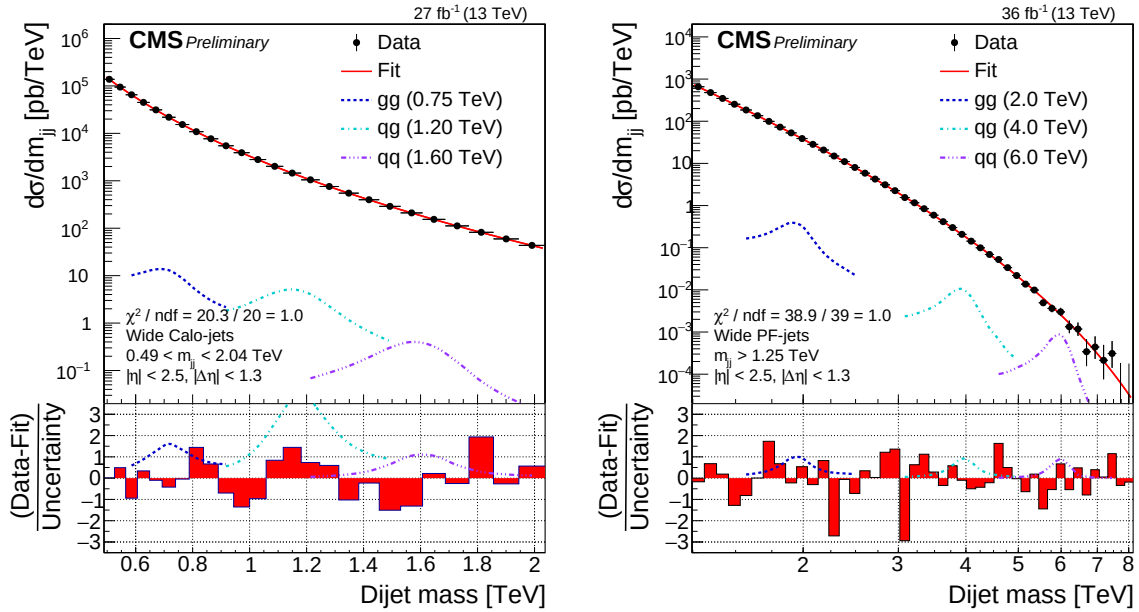

Figure 1: Dijet mass spectra (points) compared to a fitted parameterization of the background (solid curve) for the low-mass search (left) and the high-mass search (right). The lower panel in each plot shows the difference between the data and the fitted parametrization, divided by the statistical uncertainty of the data. Examples of predicted signals from narrow gluon-gluon, quark-gluon, and quark-quark resonances are shown with cross sections equal to the observed upper limits at 95% CL.

Figure 1 shows the dijet mass spectra, defined as the observed number of events in each bin divided by the integrated luminosity and the bin width, with predefined bins of width corresponding to the dijet mass resolution [16]. The dijet mass spectrum for the high-mass search is fit with the parameterization

$$\frac{\mathrm{d}\sigma}{\mathrm{d}m_{\mathrm{jj}}} = \frac{P_0(1-x)^{P_1}}{x^{P_2+P_3\ln(x)}}\,, \tag{1}$$

where $x = m_{\mathrm{jj}}/\sqrt{s}$ and P_0, P_1, P_2, and P_3 are four free parameters, and the chi-squared per number of degrees of freedom of the fit is $\chi^2/\mathrm{NDF} = 38.9/39$. The functional form in Eq. (1) was also used in previous searches [4, 6–17, 43] to describe the data. For the low-mass search the functional form in Eq. (1) gave a poor fit to the data, $\chi^2/\mathrm{NDF} = 27.9/21$, so we used the following parameterization which includes one additional parameter P_4 to fit the dijet mass spectrum:

$$\frac{\mathrm{d}\sigma}{\mathrm{d}m_{\mathrm{jj}}} = \frac{P_0(1-x)^{P_1}}{x^{P_2+P_3\ln(x)+P_4\ln(x)^2}} \tag{2}$$

Equation (2) gave a good fit to the low-mass data, $\chi^2/\mathrm{NDF} = 20.3/20$. A Fisher F-test with a size $\alpha = 0.05$ [44] was used to confirm that no additional parameters are needed to model these distributions, *i.e.* in the low-mass search including an additional term $P_5\ln(x)^3$ in Eq.(2) gave a similar fit to the low-mass data, $\chi^2/\mathrm{NDF} = 20.1/19$, and was rejected by the Fisher F-test. In Fig. 1 we show the result of binned maximum likelihood fits, performed independently for the low-mass and high-mass searches. The dijet mass spectra are well modeled by the background fits. The lower panels of Fig. 1 shows the pulls of the fit, which are the bin-by-bin differences

between the data and the background fit divided by the statistical uncertainty of the data. In the region of dijet mass between 1.2 and 2.0 TeV, the pulls of the fit are not identical in the two searches because fluctuations in reconstructed dijet mass for Calo-jets and PF-jets are not completely correlated.

Figure 1 also shows examples of dijet mass distributions for signal events generated with the PYTHIA 8.205 [45] program with the CUETP8M1 tune [46, 47] and including a GEANT4-based [48] simulation of the CMS detector. The quark-quark (qq) resonances are modeled by $q\bar{q} \to G \to q\bar{q}$, the quark-gluon (qg) resonances are modeled by $qg \to q^* \to qg$, and the gluon-gluon (gg) resonances are modeled by $gg \to G \to gg$. The predicted mass distributions have Gaussian cores from jet energy resolution, and tails towards lower mass values primarily from QCD radiation. The contribution of the low mass tail to the lineshape depends on the parton content of the resonance (qq, qg, or gg). Resonances containing gluons, which emit more QCD radiation than quarks, are wider and have a more pronounced tail. The signal distributions shown in Fig. 1 are for qq, qg, and gg resonances with signal cross sections corresponding to the limits at 95% confidence level (CL) obtained by this analysis, as described below. There is no evidence for a narrow resonance in the data. The most significant excess of the data relative to the background-only fit with the default fitting function (Eq. 1 or Eq. 2) comes from the two consecutive bins between 0.79 and 0.89 TeV. Fitting these data to qq, qg, and gg resonances with a mass of 0.85 TeV yields local significances of 1.3, 1.6 and 1.9 standard deviations including systematic uncertainties, respectively.

Signal injection tests were performed to investigate the potential bias introduced through the choice of background parameterization. Pseudo-data generated assuming two alternative parameterizations, $\mathrm{d}\sigma/\mathrm{d}m_{jj} = P_0 \exp(P_1 x^{P_2} + P_3(1-x)^{P_4})$ and $\mathrm{d}\sigma/\mathrm{d}m_{jj} = (P_0/x^{P_1}) \exp(-P_2 x - P_3 x^2 - P_4 x^3)$, were fit with the nominal parameterization given in Eq. (2). The bias in the extracted signal was found to be negligible.

4 Limits on dijet resonances

We use the dijet mass spectrum from wide jets, the background parameterization, and the dijet resonance shapes to set limits on the production of new particles decaying to the parton pairs qq (or $q\bar{q}$), qg, and gg. A separate limit is determined for each final state (qq, qg, and gg) because of the dependence of the dijet resonance shape on the types of the two final-state partons.

The dominant sources of systematic uncertainty are the jet energy scale and resolution, integrated luminosity, and the value of the parameters within the functional form modeling the background shape in the dijet mass distribution. The uncertainty in the jet energy scale in both the low-mass and the high-mass search is 2% and is determined from $\sqrt{s} = 13$ TeV data using the methods described in Ref. [41]. This uncertainty is propagated to the limits by shifting the dijet mass shape for signal by $\pm 2\%$. The uncertainty in the jet energy resolution translates into an uncertainty of 10% in the resolution of the dijet mass [41], and is propagated to the limits by observing the effect of increasing and decreasing by 10% the reconstructed width of the dijet mass shape for signal. The uncertainty in the integrated luminosity is 2.6%, and is propagated to the normalization of the signal. Changes in the values of the parameters describing the background introduce a change in the signal strength, which is accounted for as a systematic uncertainty as discussed in the next paragraph.

The modified frequentist method [49, 50] is utilized to set upper limits on signal cross sections, following the prescription described in Refs. [51, 52]. We use a multi-bin counting experi-

ment likelihood, which is a product of Poisson distributions corresponding to different bins. We evaluate the likelihood independently at each value of resonance pole mass from 0.6 to 1.6 TeV in 50-GeV steps in the low-mass search, and from 1.6 to 8.1 TeV in 100-GeV steps in the high-mass search. The systematic uncertainties are implemented as nuisance parameters in the likelihood model, with Gaussian constraints for the jet energy scale and resolution, and log-normal constraints for the integrated luminosity. The systematic uncertainty in the background is automatically evaluated via profiling, effectively refitting for the optimal values of the background parameters for each value of resonance cross section. The extent to which the background uncertainty affects the limit depends significantly on the signal shape and the resonance mass, with the largest effect occurring for the gg resonances because they are wider, and the smallest effect for qq resonances. The effect decreases as the resonance mass increases.

Figures 2 and 3 show the model-independent observed upper limits at 95% CL on the product of the cross section (σ), the branching fraction (B), and the acceptance (A) for narrow resonances, with the kinematic requirements $|\Delta\eta_{jj}| < 1.3$ and $|\eta| < 2.5$. The acceptance of the minimum dijet mass requirement in each search has been evaluated separately for qq, qg, and gg resonances, and has been taken into account by correcting the limits, and therefore does not appear in the acceptance A. The resonance mass boundary of 1.6 TeV between the high and low mass search was chosen to maintain a reasonable acceptance for the minimum dijet mass requirement imposed by the high mass search. For a 1.6 TeV dijet resonance, the acceptance of the 1.25 TeV dijet mass requirement is 57% for a gluon-gluon resonance, 76% for a quark-gluon resonance, and 85% for a quark-quark resonance. Figure 2 also shows the expected limits on $\sigma\, B\, A$ and their bands of uncertainty. The difference in the limits for qq, qg, and gg resonances at the same resonance mass originates from the difference in their lineshapes. For the RS graviton model, which decays to both $q\bar{q}$ and gg, we obtain cross section upper limits from the branching fraction weighted average of the limits on quark-quark and gluon-gluon resonances.

All upper limits presented can be compared to the parton-level predictions of $\sigma\, B\, A$, without detector simulation, to determine mass limits on new particles. The model predictions shown in Figs. 2 and 3 are calculated in the narrow-width approximation [18] using the CTEQ6L1 [53] PDF at leading order, with a next-to-leading order correction factor of approximately 1.3 included for the W′ and Z′ models, and approximately 1.2 for the axigluon/coloron models [24]. The branching fraction includes the direct decays of the resonance into the five light quarks and gluons only, excluding top quarks from the decay, although top quarks are included in the calculation of the resonance width. The acceptance is evaluated at the parton level for the resonance decay to two partons. In the case of isotropic decays, the acceptance is $A \approx 0.6$ and is independent of the resonance mass. For a given model, new particles are excluded at 95% CL in mass regions where the theoretical prediction lies at or above the observed upper limit for the appropriate final state of Figs. 2 and 3. Mass limits on all benchmark models are summarized in Table 1 and are more stringent than the mass limits in the dijet channel previously reported by CMS [3] and ATLAS [5].

Mass limits on new particles are sensitive to assumptions about their coupling. Conversely, at a fixed resonance mass, models with smaller couplings are excluded by searches with increased sensitivity. Figure 4 shows upper limits on the coupling as a function of mass for a model of a leptophobic Z′ resonance with a universal quark coupling, g'_q [30], related to the Z′ coupling convention of Ref. [54] by $g'_q = g_B/6$.

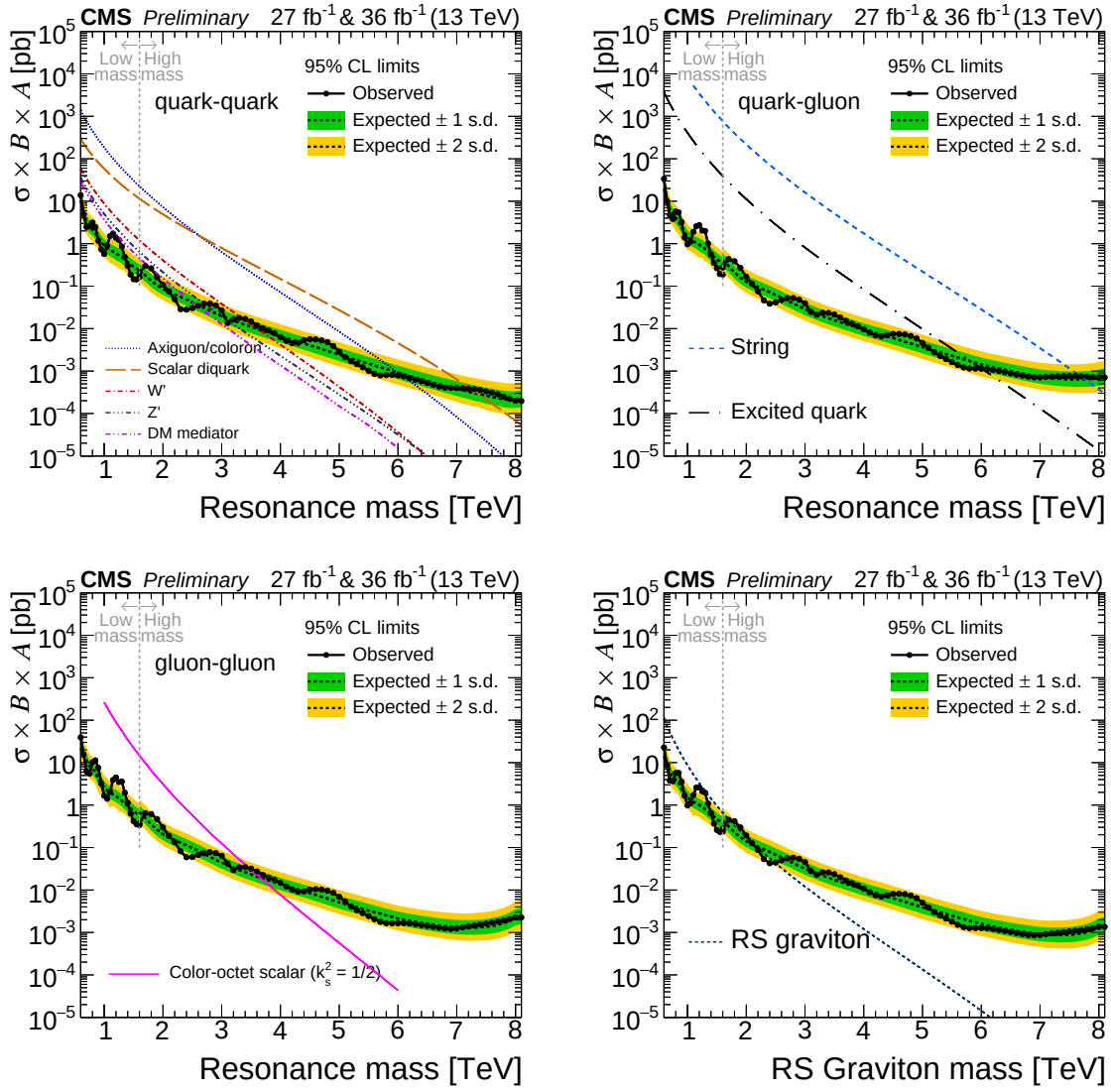

Figure 2: The observed 95% CL upper limits on the product of the cross section, branching fraction, and acceptance for dijet resonances decaying to quark-quark (top left), quark-gluon (top right), gluon-gluon (bottom left), and for RS gravitons (bottom right). The corresponding expected limits (dashed) and their variations at the 1 and 2 standard deviation levels (shaded bands) are also shown. Limits are compared to predicted cross sections for string resonances [20, 21], excited quarks [26, 27], axigluons [23], colorons [25], scalar diquarks [22], color-octet scalars [28], new gauge bosons W' and Z' with SM-like couplings [29], dark matter mediators for $m_{\mathrm{DM}} = 1\,\mathrm{GeV}$ [30, 31], and RS gravitons [32].

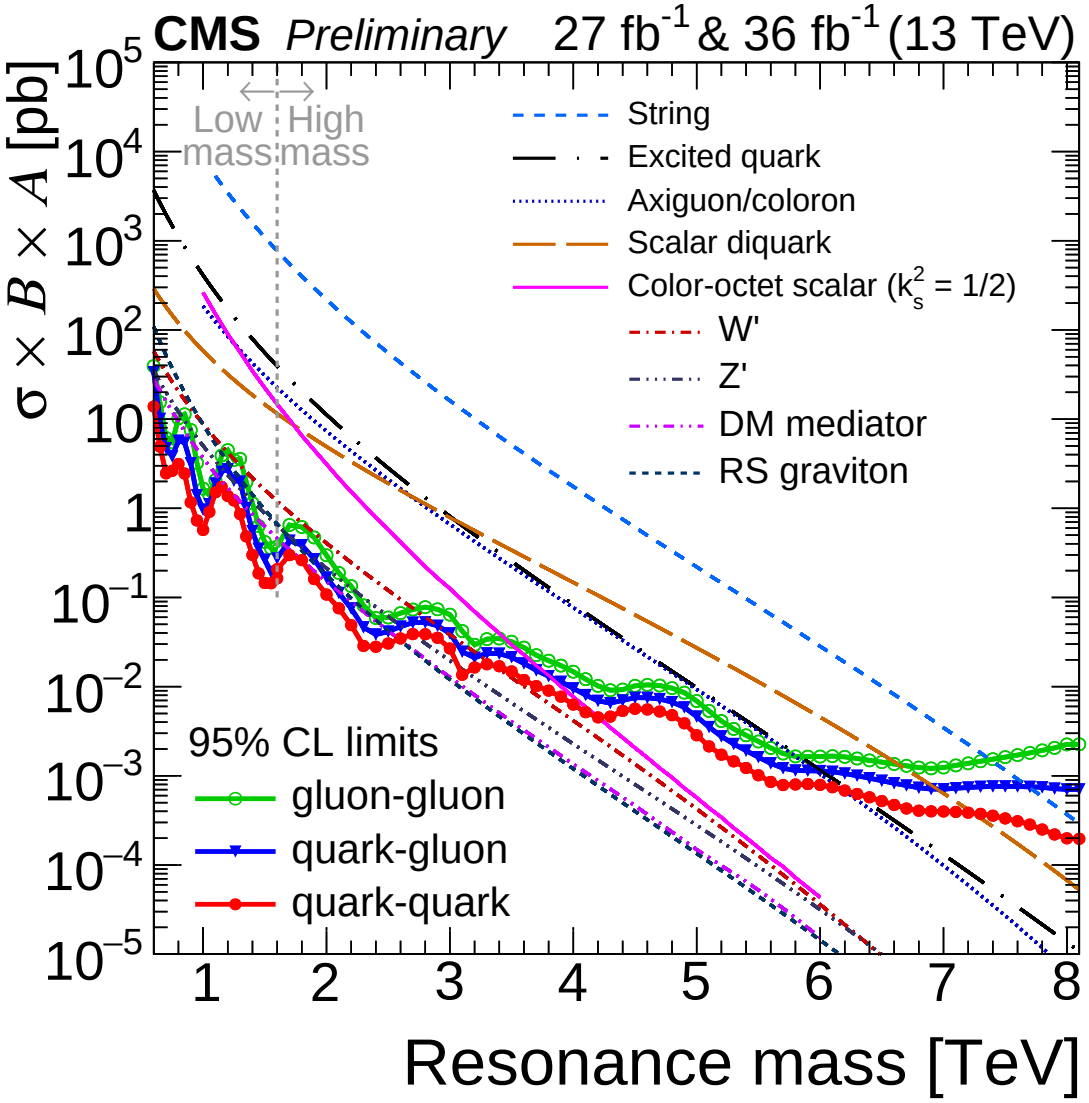

Figure 3: The observed 95% CL upper limits on the product of the cross section, branching fraction, and acceptance for quark-quark, quark-gluon, and gluon-gluon type dijet resonances. Limits are compared to predicted cross sections for string resonances [20, 21], excited quarks [26, 27], axigluons [23], colorons [25], scalar diquarks [22], color-octet scalars [28], new gauge bosons W′ and Z′ with SM-like couplings [29], dark matter mediators for $m_{\mathrm{DM}} = 1\,\mathrm{GeV}$ [30, 31], and RS gravitons [32].

Table 1: Observed and expected mass limits at 95% CL from this analysis with 36 fb^{-1} at $\sqrt{s} =$ 13 TeV compared to previously published limits on narrow resonances from CMS with 12.9 fb^{-1} and 2.4 fb^{-1} at $\sqrt{s} = 13$ TeV [3, 6] and with 20 fb^{-1} at $\sqrt{s} = 8$ TeV [8]. The listed models are excluded between 0.6 TeV and the indicated mass limit by this analysis. In addition to the observed mass limits listed below, this analysis also excludes the RS Graviton model within the mass interval between 2.1 and 2.5 TeV and the Z′ model within roughly a 50 GeV window around 3.1 TeV.

		Observed (expected) mass limit [TeV]			
Model	Final State	36 fb^{-1} 13 TeV	12.9 fb^{-1} 13 TeV	2.4 fb^{-1} 13 TeV	20 fb^{-1} 8 TeV
String	qg	7.7 (7.7)	7.4 (7.4)	7.0 (6.9)	5.0 (4.9)
Scalar diquark	qq	7.2 (7.4)	6.9 (6.8)	6.0 (6.1)	4.7 (4.4)
Axigluon/coloron	$\text{q}\bar{\text{q}}$	6.1 (6.0)	5.5 (5.6)	5.1 (5.1)	3.7 (3.9)
Excited quark	qg	6.0 (5.8)	5.4 (5.4)	5.0 (4.8)	3.5 (3.7)
Color-octet scalar ($k_s^2 = 1/2$)	gg	3.4 (3.6)	3.0 (3.3)	—	—
W′	$\text{q}\bar{\text{q}}$	3.3 (3.6)	2.7 (3.1)	2.6 (2.3)	2.2 (2.2)
Z′	$\text{q}\bar{\text{q}}$	2.7 (2.9)	2.1 (2.3)	—	1.7 (1.8)
RS Graviton ($k/M_{\text{PL}} = 0.1$)	$\text{q}\bar{\text{q}}$, gg	1.7 (2.1)	1.9 (1.8)	—	1.6 (1.3)
DM Mediator ($m_{\text{DM}} = 1$ GeV)	$\text{q}\bar{\text{q}}$	2.6 (2.5)	2.0 (2.0)	—	—

5 Limits on dark matter

We use our limits to constrain simplified models of DM, with leptophobic vector and axial-vector mediators that couple only to quarks and DM particles [30, 31]. Figure 5 shows the excluded values of mediator mass as a function of m_{DM} for both types of mediators. For m_{DM} = 1 GeV, indistinguishable from zero, the observed excluded range of mediator mass (M_{Med}) is between 0.6 and 2.6 TeV, as also shown in Fig. 2 and listed in Table 1. In Fig. 5 the expected upper value of excluded M_{Med} increases with m_{DM} because the branching fraction to $\text{q}\bar{\text{q}}$ increases with m_{DM}. If $m_{\text{DM}} > M_{\text{Med}}/2$, the mediator cannot decay to DM particles, and the dijet cross section from the mediator models becomes identical to that in the leptophobic Z′ model used in Fig. 4 with a coupling $g'_{\text{q}} = g_{\text{q}} = 0.25$. Therefore for these values of m_{DM} the limits on the mediator mass in Fig. 5 are identical to the limits on the Z′ mass at $g'_{\text{q}} = 0.25$ in Fig. 4. Similarly, if $m_{\text{DM}} = 0$, the limits on the mediator mass in Fig. 5 are identical to the limits on the Z′ mass at $g'_{\text{q}} = g_{\text{q}}/\sqrt{1 + 16/(3N_f)} \approx 0.182$ in Fig. 4, where N_f is the effective number of quark flavors contributing to the width of the resonance, $N_f = 5 + \sqrt{1 - 4m_t^2/M_{\text{Med}}^2}$. In Fig. 5 our exclusions are compared to constraints from the cosmological relic density of DM.

6 Summary

Two searches for narrow resonances decaying into a pair of jets have been performed using proton-proton collisions at $\sqrt{s} = 13$ TeV corresponding to an integrated luminosity of up to 36 fb^{-1}: a low-mass search based on calorimeter jets, reconstructed by the high level trigger and recorded in compact form (data scouting), and a high-mass search based on particle-flow jets. The dijet mass spectra are observed to be smoothly falling distributions. In the analyzed data samples, there is no evidence for resonant particle production. Generic upper limits are presented on the product of the cross section, the branching fraction, and the acceptance for narrow quark-quark, quark-gluon, and gluon-gluon resonances that are applicable to any model

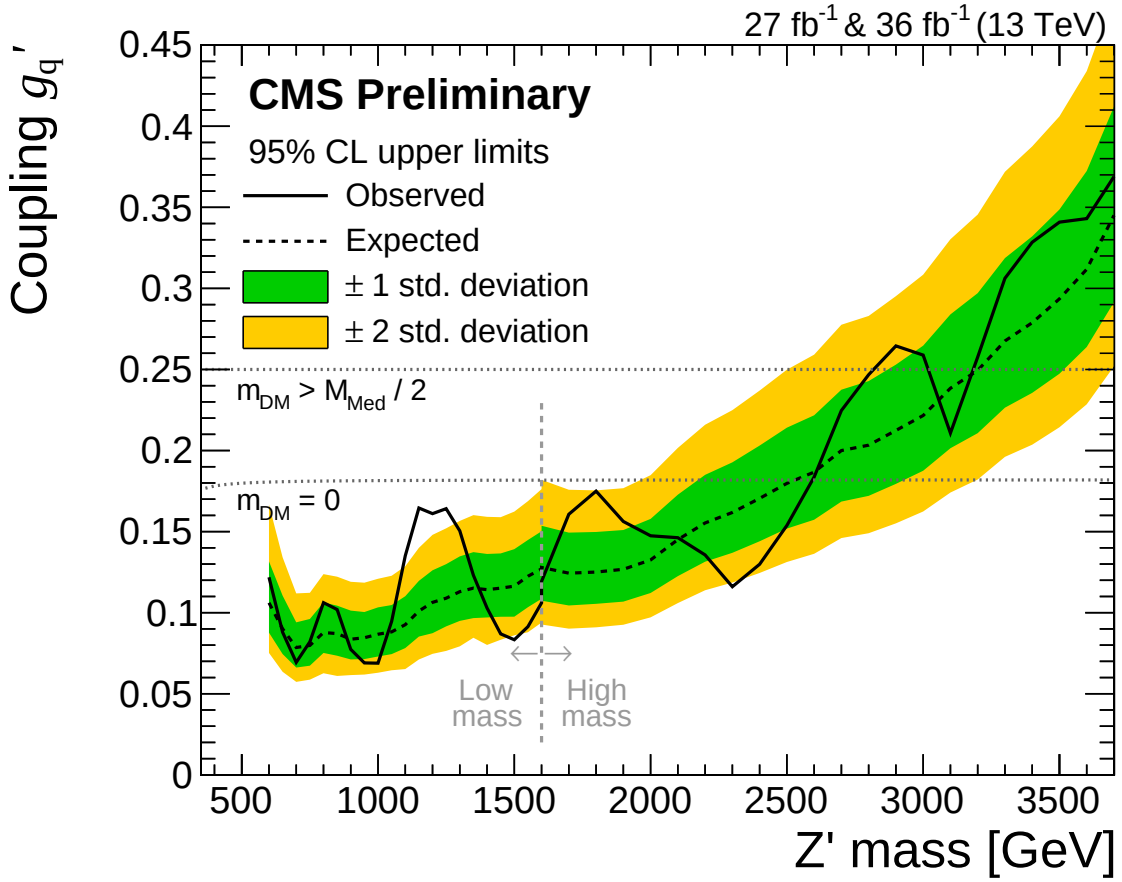

Figure 4: The 95% CL upper limits on the universal quark coupling g'_q as a function of resonance mass for a leptophobic Z′ resonance that only couples to quarks. The observed limits (solid), expected limits (dashed) and their variation at the 1 and 2 standard deviation levels (shaded bands) are shown. Dotted horizontal lines show the coupling strength for which the cross section for dijet production in this model is the same as for a DM mediator (see text).

of narrow dijet resonance production. String resonances with masses below 7.7 TeV are excluded at 95% confidence level, as are scalar diquarks below 7.2 TeV, axigluons and colorons below 6.1 TeV, excited quarks below 6.0 TeV, color-octet scalars below 3.4 TeV, W′ bosons below 3.3 TeV, Z′ bosons with SM-like couplings below 2.7 TeV, and Randall–Sundrum gravitons below 1.7 TeV and between 2.1 and 2.5 TeV, and dark matter mediators below 2.6 TeV. The limits on both vector and axial-vector mediators, in a simplified model of interactions between quarks and dark matter, are also presented as functions of dark matter mass. This extends previously reported limits in the dijet channel.

References

[1] M. Chala et al., "Constraining dark sectors with monojets and dijets", *JHEP* **07** (2015) 089, doi:10.1007/JHEP07(2015)089, arXiv:1503.05916.

[2] CMS Collaboration, "Data Parking and Data Scouting at the CMS Experiment", CMS Detector Performance Summary CMS-DP-2012-022, 2012.

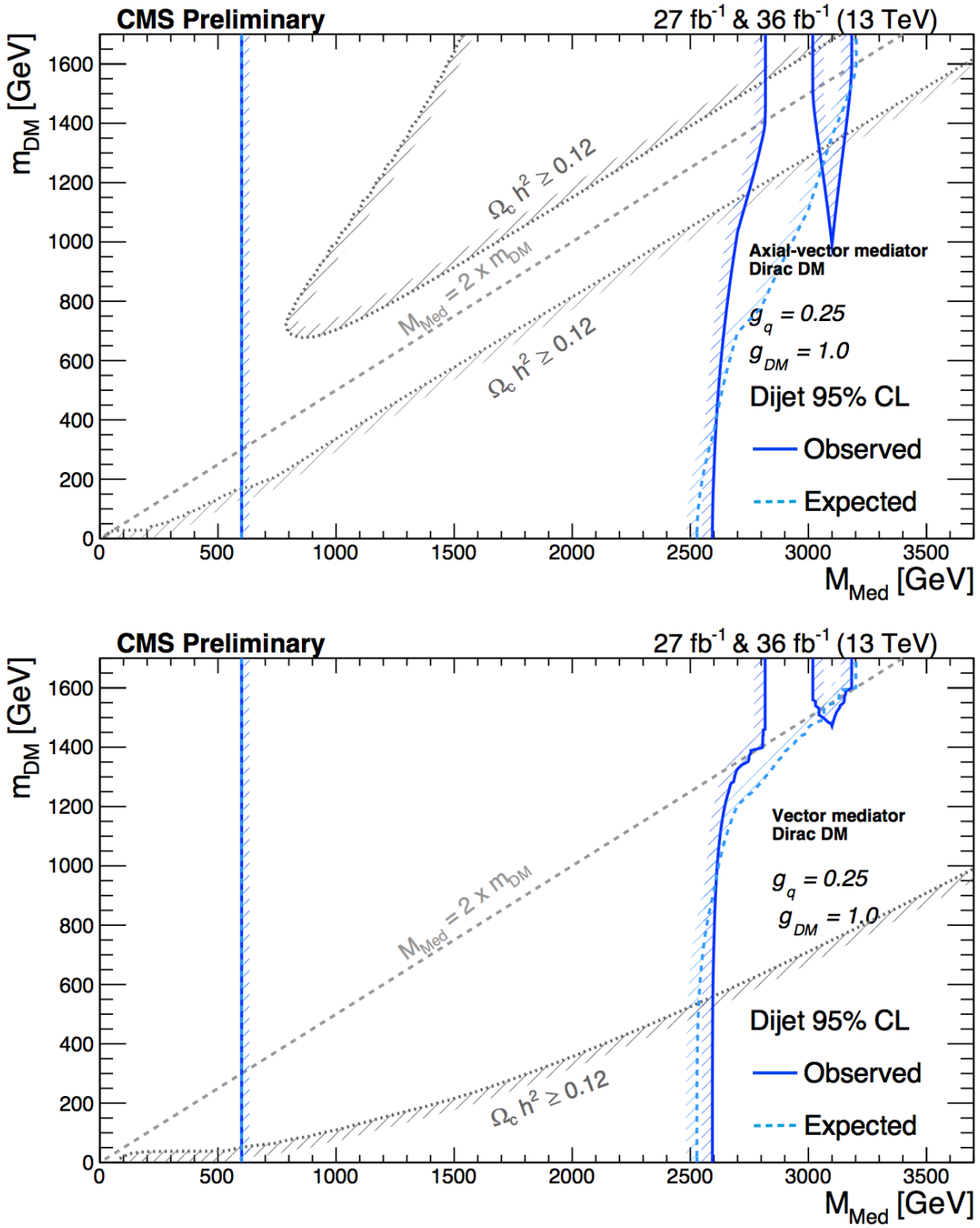

Figure 5: The 95% CL observed (solid) and expected (dashed) excluded regions in the plane of dark matter mass vs. mediator mass, for an axial-vector mediator (top) and a vector mediator (bottom), are compared to constraints from the cosmological relic density of DM (light gray) determined from astrophysical measurements [55, 56] and MADDM version 2.0.6 [57, 58] as described in Ref. [59]. Following the recommendation of the LHC DM working group [30, 31], the exclusions are computed for Dirac DM and for a universal quark coupling $g_q = 0.25$ and for a DM coupling of $g_{DM} = 1.0$. It should also be noted that the excluded region strongly depends on the chosen coupling and model scenario. Therefore, the excluded regions and relic density contours shown in this plot are not applicable to other choices of coupling values or models.

[3] CMS Collaboration, "Search for dijet resonances in proton-proton collisions at $\sqrt{s} = 13$ TeV and constraints on dark matter and other models", (2016). arXiv:1611.03568. Submitted to PLB.

[4] CMS Collaboration, "Search for Narrow Resonances in Dijet Final States at $\sqrt{s} = 8$ TeV with the Novel CMS Technique of Data Scouting", *Phys. Rev. Lett.* **117** (2016) 031802, doi:10.1103/PhysRevLett.117.031802, arXiv:1604.08907.

[5] ATLAS Collaboration, "Search for light dijet resonances with the ATLAS detector using a Trigger-object Level Analysis in LHC pp collisions at $\sqrt{s} = 13$ TeV", ATLAS Conference Report ATLAS-CONF-2016-030, Jun, 2016.

[6] CMS Collaboration, "Search for Narrow Resonances Decaying to Dijets in Proton-Proton Collisions at $\sqrt{s} = 13$ TeV", *Phys. Rev. Lett.* **116** (2016) 071801, doi:10.1103/PhysRevLett.116.071801, arXiv:1512.01224.

[7] ATLAS Collaboration, "Search for new phenomena in dijet mass and angular distributions from pp collisions at $\sqrt{s} = 13$ TeV with the ATLAS detector", *Phys. Lett. B* **754** (2016) 302, doi:10.1016/j.physletb.2016.01.032, arXiv:1512.01530.

[8] CMS Collaboration, "Search for resonances and quantum black holes using dijet mass spectra in proton-proton collisions at $\sqrt{s} = 8$ TeV", *Phys. Rev. D* **91** (2015) 052009, doi:10.1103/PhysRevD.91.052009, arXiv:1501.04198.

[9] ATLAS Collaboration, "Search for new phenomena in the dijet mass distribution using pp collision data at $\sqrt{s} = 8$ TeV with the ATLAS detector", *Phys. Rev. D* **91** (2015) 052007, doi:10.1103/PhysRevD.91.052007, arXiv:1407.1376.

[10] CMS Collaboration, "Search for narrow resonances using the dijet mass spectrum in pp collisions at $\sqrt{s} = 8$ TeV", *Phys. Rev. D* **87** (2013) 114015, doi:10.1103/PhysRevD.87.114015, arXiv:1302.4794.

[11] CMS Collaboration, "Search for narrow resonances and quantum black holes in inclusive and b-tagged dijet mass spectra from pp collisions at $\sqrt{s} = 7$ TeV", *JHEP* **01** (2013) 013, doi:10.1007/JHEP01(2013)013, arXiv:1210.2387.

[12] ATLAS Collaboration, "Search for new physics in the dijet mass distribution using 1 fb^{-1} of pp collision data at $\sqrt{s} = 7$ TeV collected by the ATLAS detector", *Phys. Lett. B* **708** (2012) 37, doi:10.1016/j.physletb.2012.01.035, arXiv:1108.6311.

[13] ATLAS Collaboration, "ATLAS search for new phenomena in dijet mass and angular distributions using pp collisions at $\sqrt{s} = 7$ TeV", *JHEP* **01** (2013) 029, doi:10.1007/JHEP01(2013)029, arXiv:1210.1718.

[14] CMS Collaboration, "Search for resonances in the dijet mass spectrum from 7 TeV pp collisions at CMS", *Phys. Lett. B* **704** (2011) 123, doi:10.1016/j.physletb.2011.09.015, arXiv:1107.4771.

[15] ATLAS Collaboration, "Search for new physics in dijet mass and angular distributions in pp collisions at $\sqrt{s} = 7$ TeV measured with the ATLAS detector", *New J. Phys.* **13** (2011) 053044, doi:10.1088/1367-2630/13/5/053044, arXiv:1103.3864.

[16] CMS Collaboration, "Search for Dijet Resonances in 7 TeV pp Collisions at CMS", *Phys. Rev. Lett.* **105** (2010) 211801, doi:10.1103/PhysRevLett.105.211801, arXiv:1010.0203. [Erratum doi:10.1103/PhysRevLett.106.029902].

[17] ATLAS Collaboration, "Search for New Particles in Two-Jet Final States in 7 TeV Proton-Proton Collisions with the ATLAS Detector at the LHC", *Phys. Rev. Lett.* **105** (2010) 161801, doi:10.1103/PhysRevLett.105.161801, arXiv:1008.2461.

[18] R. M. Harris and K. Kousouris, "Searches for dijet resonances at hadron colliders", *Int. J. Mod. Phys. A* **26** (2011) 5005, doi:10.1142/S0217751X11054905, arXiv:1110.5302.

[19] ATLAS Collaboration, "Search for New Phenomena in Dijet Events with the ATLAS Detector at $\sqrt{s}$=13 TeV with 2015 and 2016 data", ATLAS Conference Report ATLAS-CONF-2016-069, Aug, 2016.

[20] L. A. Anchordoqui et al., "Dijet Signals for Low Mass Strings at the LHC", *Phys. Rev. Lett.* **101** (2008) 241803, doi:10.1103/PhysRevLett.101.241803, arXiv:0808.0497.

[21] S. Cullen, M. Perelstein, and M. E. Peskin, "TeV strings and collider probes of large extra dimensions", *Phys. Rev. D* **62** (2000) 055012, doi:10.1103/PhysRevD.62.055012, arXiv:hep-ph/0001166.

[22] J. L. Hewett and T. G. Rizzo, "Low-energy phenomenology of superstring-inspired E(6) models", *Phys. Rept.* **183** (1989) 193, doi:10.1016/0370-1573(89)90071-9.

[23] P. H. Frampton and S. L. Glashow, "Chiral Color: An Alternative to the Standard Model", *Phys. Lett. B* **190** (1987) 157, doi:10.1016/0370-2693(87)90859-8.

[24] R. S. Chivukula, E. H. Simmons, A. Farzinnia, and J. Ren, "Hadron collider production of massive color-octet vector bosons at next-to-leading order", *Phys. Rev. D* **87** (2013) 094011, doi:10.1103/PhysRevD.87.094011, arXiv:1303.1120.

[25] E. H. Simmons, "Coloron phenomenology", *Phys. Rev. D* **55** (1997) 1678, doi:10.1103/PhysRevD.55.1678, arXiv:hep-ph/9608269.

[26] U. Baur, I. Hinchliffe, and D. Zeppenfeld, "Excited Quark Production at Hadron Colliders", *Int. J. Mod. Phys. A* **02** (1987) 1285, doi:10.1142/S0217751X87000661.

[27] U. Baur, M. Spira, and P. M. Zerwas, "Excited quark and lepton production at hadron colliders", *Phys. Rev. D* **42** (1990) 815, doi:10.1103/PhysRevD.42.815.

[28] T. Han, I. Lewis, and Z. Liu, "Colored resonant signals at the LHC: largest rate and simplest topology", *JHEP* **12** (2010) 085, doi:10.1007/JHEP12(2010)085, arXiv:1010.4309.

[29] E. Eichten, I. Hinchliffe, K. D. Lane, and C. Quigg, "Supercollider physics", *Rev. Mod. Phys.* **56** (1984) 579, doi:10.1103/RevModPhys.56.579.

[30] A. Boveia et al., "Recommendations on presenting LHC searches for missing transverse energy signals using simplified *s*-channel models of dark matter", (2016). arXiv:1603.04156.

[31] J. Abdallah et al., "Simplified models for dark matter searches at the LHC", *Phys. Dark Univ.* **9-10** (2015) 8, doi:10.1016/j.dark.2015.08.001, arXiv:1506.03116.

[32] L. Randall and R. Sundrum, "An alternative to compactification", *Phys. Rev. Lett.* **83** (1999) 4690, doi:10.1103/PhysRevLett.83.4690, arXiv:hep-th/9906064.

[33] R. S. Chivukula, E. H. Simmons, and N. Vignaroli, "Distinguishing dijet resonances at the LHC", *Phys. Rev. D* **91** (2015) 055019, doi:10.1103/PhysRevD.91.055019, arXiv:1412.3094.

[34] CMS Collaboration, "The CMS experiment at the CERN LHC", *JINST* **3** (2008) S08004, doi:10.1088/1748-0221/3/08/S08004.

[35] CMS Collaboration, "Particle–Flow Event Reconstruction in CMS and Performance for Jets, Taus, and $E_{\mathrm{T}}^{\mathrm{miss}}$", CMS Physics Analysis Summary CMS-PAS-PFT-09-001, 2009.

[36] CMS Collaboration, "Commissioning of the Particle-flow Event Reconstruction with the first LHC collisions recorded in the CMS detector", CMS Physics Analysis Summary CMS-PAS-PFT-10-001, 2010.

[37] M. Cacciari, G. P. Salam, and G. Soyez, "The Anti-k_{t} jet clustering algorithm", *JHEP* **04** (2008) 063, doi:10.1088/1126-6708/2008/04/063, arXiv:0802.1189.

[38] M. Cacciari and G. P. Salam, "Dispelling the N^3 myth for the k_{t} jet-finder", *Phys. Lett. B* **641** (2006) 57, doi:10.1016/j.physletb.2006.08.037, arXiv:hep-ph/0512210.

[39] M. Cacciari, G. P. Salam, and G. Soyez, "FastJet user manual", *Eur. Phys. J. C* **72** (2012) 1896, doi:10.1140/epjc/s10052-012-1896-2, arXiv:1111.6097.

[40] M. Cacciari and G. P. Salam, "Pileup subtraction using jet areas", *Phys. Lett. B* **659** (2008) 119, doi:10.1016/j.physletb.2007.09.077, arXiv:0707.1378.

[41] CMS Collaboration, "Jet energy scale and resolution in the CMS experiment in pp collisions at 8 TeV", (2016). arXiv:1607.03663. Submitted to JINST.

[42] CMS Collaboration, "Jet Performance in pp Collisions at $\sqrt{s} = 7$ TeV", CMS Physics Analysis Summary CMS-PAS-JME-10-003, 2010.

[43] CDF Collaboration, "Search for new particles decaying into dijets in proton-antiproton collisions at $\sqrt{s} = 1.96$ TeV", *Phys. Rev. D* **79** (2009) 112002, doi:10.1103/PhysRevD.79.112002, arXiv:0812.4036.

[44] R. G. Lomax and D. L. Hahs-Vaughn, "Statistical concepts: A second course". Routledge Academic, London, 2007.

[45] T. Sjöstrand, S. Mrenna, and P. Skands, "A brief introduction to PYTHIA 8.1", *Comp. Phys. Comm.* **178** (2008) 852, doi:10.1016/j.cpc.2008.01.036, arXiv:0710.3820.

[46] CMS Collaboration, "Event generator tunes obtained from underlying event and multiparton scattering measurements", *Eur. Phys. J. C* **76** (2016) 155, doi:10.1140/epjc/s10052-016-3988-x, arXiv:1512.00815.

[47] P. Skands, S. Carrazza, and J. Rojo, "Tuning PYTHIA 8.1: the Monash 2013 tune", *Eur. Phys. J. C* **74** (2014) 3024, doi:10.1140/epjc/s10052-014-3024-y, arXiv:1404.5630.

[48] GEANT4 Collaboration, "GEANT4 — a simulation toolkit", *Nucl. Instrum. Meth. A* **506** (2003) 250, doi:10.1016/S0168-9002(03)01368-8.

[49] T. Junk, "Confidence level computation for combining searches with small statistics", *Nucl. Instr. Meth. A* **434** (1999) 435, doi:10.1016/S0168-9002(99)00498-2, arXiv:hep-ex/9902006.

[50] A. L. Read, "Presentation of search results: the CL_s technique", *J. Phys. G* **28** (2002) 2693, doi:10.1088/0954-3899/28/10/313.

[51] LHC Higgs Combination Group, "Procedure for the LHC Higgs boson search combination in Summer 2011", Technical Report CMS-NOTE-2011-005, ATL-PHYS-PUB-2011-11, 2011.

[52] G. Cowan, K. Cranmer, E. Gross, and O. Vitells, "Asymptotic formulae for likelihood-based tests of new physics", *Eur. Phys. J. C* **71** (2011) 1554, doi:10.1140/epjc/s10052-011-1554-0, arXiv:1007.1727. [Erratum: doi:10.1140/epjc/s10052-013-2501-z].

[53] J. Pumplin et al., "New generation of parton distributions with uncertainties from global QCD analysis", *JHEP* **07** (2002) 012, doi:10.1088/1126-6708/2002/07/012, arXiv:hep-ph/0201195.

[54] B. A. Dobrescu and F. Yu, "Coupling-mass mapping of dijet peak searches", *Phys. Rev. D* **88** (2013) 035021, doi:10.1103/PhysRevD.88.035021, arXiv:1306.2629. [Erratum: doi:10.1103/PhysRevD.90.079901].

[55] WMAP Collaboration, "Wilkinson Microwave Anisotropy Probe (WMAP) three year results: implications for cosmology", *Astrophys. J. Suppl.* **170** (2007) 377, doi:10.1086/513700, arXiv:astro-ph/0603449.

[56] Planck Collaboration, "Planck 2013 results. XVI. Cosmological parameters", *Astron. Astrophys.* **571** (2014) A16, doi:10.1051/0004-6361/201321591, arXiv:1303.5076.

[57] M. Backovic, K. Kong, and M. McCaskey, "MadDM v.1.0: Computation of Dark Matter Relic Abundance Using MadGraph5", *Phys. Dark Univ.* **5** (2014) 18, doi:10.1016/j.dark.2014.04.001, arXiv:1308.4955.

[58] M. Backovic et al., "Direct detection of dark matter with MadDM v.2.0", *Phys. Dark Univ.* **9** (2015) 37, doi:10.1016/j.dark.2015.09.001, arXiv:1505.04190.

[59] T. du Pree, K. Hahn, P. Harris, and C. Roskas, "Cosmological constraints on Dark Matter models for collider searches", (2016). arXiv:1603.08525.